

High Galactic Latitude Interstellar Neutral Hydrogen Structure and Associated (WMAP) High Frequency Continuum Emission

Gerrit L. Verschuur

Physics Department, University of Memphis, Memphis, TN 38152 gverschr@memphis.edu

Received _____; accepted _____

Revised, February 7, 2007

arXiv:0704.1125v1 [astro-ph] 9 Apr 2007

ABSTRACT

Spatial associations have been found between interstellar neutral hydrogen (HI) emission morphology and small-scale structure observed by the *Wilkinson Microwave Anisotropy Probe (WMAP)* in a Target Area bounded by $l = 60^\circ$ & 180° , $b = 30^\circ$ & 70° . This area is marked by the presence of highly disturbed local HI and a preponderance of intermediate- and high-velocity gas and it remains to be determined whether the claimed associations are a hallmark of the presence of the anomalous velocity gas. The HI distribution toward the 33 brightest *WMAP* peaks in the Target Area is examined and it is demonstrated that the associations do not appear to be the result of chance coincidence. Furthermore, several important properties of diffuse interstellar neutral hydrogen structure have been identified that might otherwise have been overlooked if it were not for the fact that the continuum data focused attention on certain areas of the HI sky. Some of the most dramatic associations are illustrated. It is suggested that continuum emission is produced at the interface between interacting (colliding) HI structures or at the interface between moving HI structures and regions of enhanced plasma density in the surrounding interstellar medium. In the case of high-velocity cloud MI, HI and *WMAP* morphologies are clearly associated and both excess soft X-ray emission and $H\alpha$ emission have been reported at the same location. The primary purpose of this report is to draw attention to these associations in the hope that it will stimulate further research to identify the physical mechanism(s) responsible. This type of study should be extended to other high-latitude regions to determine how much, if any, of the small-scale structure observed by *WMAP* (and by implication, *COBE*) remains to be assigned a cosmological origin.

Subject headings: Interstellar matter, neutral hydrogen, cosmology, WMAP

1. Introduction

Examination of the *Wilkinson Microwave Anisotropy Probe (WMAP)* images immediately fires the imagination, especially the summary image that has received so much publicity, sometimes referred to as the *Internal Linear Combination (ILC)* map (Hinshaw et al, 2006). That map (readily accessed at <http://map.gsfc.nasa.gov>) was produced after subtraction of suspected galactic components from the 5-channel observations carried out by *WMAP*. But do those signals truly reveal the fingerprints of processes that took place shortly after the universe was born?

Upon closer inspection, certain features in the *WMAP* maps look hauntingly familiar to those who have spent their careers studying the HI structure and radio emission from the Milky Way galaxy. For example, a striking area of excess continuum emission in the *WMAP* map is found around galactic longitude (l) 140° where low frequency background polarization data show excess polarization indicating a highly ordered local magnetic field (Brouw & Spoelstra, 1976). The distinct similarity between galactic HI features and some of the *WMAP* structure can be recognized in a visual comparison of the above-referenced *WMAP* image and the all-sky HI column density map found at <http://www.astro.uni-bonn.de>. Several extended features at high galactic latitudes ($b > 30^\circ$) are present in both maps; for example in the areas around galactic longitude and latitude $(l, b) = (170^\circ, 80^\circ)$ and $(l, b) = (160^\circ, -35^\circ)$. Most striking is the extended *WMAP* structure that reaches from $(l, b) = (240^\circ, 0^\circ)$ to $(l, b) = (300^\circ, -35^\circ)$, which has a counterpart in the HI data where a tongue of emission follows the same axis, emerging from the galactic disk HI at $(l, b) = (270^\circ, -15^\circ)$ and stretching to $(l, b) = (345^\circ, -35^\circ)$. This structure was already evident in HI data shown by Fejes & Wesselius (1973).

Clearly, if the *WMAP* small-scale structure data correspond to cosmological signals, absolutely no associations with HI structure, other than those due to pure chance, should

be found. However, the apparent associations noted above were tantalizing enough to initiate a more detailed comparison between HI structure and continuum emission data for an area of sky (hereafter the Target Area) for which HI area maps at many velocities were prepared. The relevant *ILC* data were provided in digital form by the *WMAP* team at the Goddard Space Flight Center (in February 2006). For the Target Area the structure in the *ILC* summary map is morphologically the same as in any of the five frequency maps produced by *WMAP* (as is readily seen by comparing the maps on the *WMAP* web site) and thus we focus here on structural similarities between the *ILC* and HI structure.

In §2 an overview of the data is presented. In §3 data are given on the number of direct associations as well as closely offset structures found when comparing the HI and *WMAP* continuum emission maps for the Target Area contrasted with the results for a Comparison Area located symmetrically with respect to the galactic anti-center. In §4 a more formal attempt it is offered to argue that the associations are not due to chance. In §5 specific examples of one-to-one correspondence as well as close morphological associations between HI and *WMAP* continuum emission structures are considered. In the discussion in §6 suggestions regarding a possible model for producing the identified associations are described. Section 7 offers brief comments on the angular power spectrum of both types of data. In the conclusions in §8 the hope is expressed that others will be motivated to seek confirmation (or otherwise) of the claims made here. An initial report of this work is found in Verschuur (2007).

2. Data

The goal of the present study was to determine if parallels exist between galactic HI structure and high-frequency continuum emission features observed by *WMAP*. A Target Area bounded by $l = 60^\circ$ & 180° , $b = 30^\circ$ & 70° was the focus of this phase of the work.

Neutral hydrogen (HI) emission profile data with an angular resolution of 0.6° were obtained from the Leiden-Dwingeloo, sidelobe-corrected HI Survey (Hartmann & Burton, 1997) as well as the more extensive Leiden-Argentina-Bonn (LAB) All-Sky HI Survey (Kalberla et al. 2005).

The study of interstellar neutral hydrogen gas, by tradition, is divided into three categories: (1) Low Velocity (LV) gas is defined to be in the range 30 km/s with respect to the local standard of rest; (2) Intermediate Velocity (IV) gas between -30 & -100 km/s; and (3) High Velocity (HV) HI with a velocity < -100 km/s. A recent review of IV HI has been given by Albert & Danly (2004), and a review of HV HI by Wakker (2004). Although Blaauw & Tolbert (1966) suggested a relationship between the presence of IV gas and a deficiency of LV gas, it is striking that the recent literature has evolved to become ever more compartmentalized, with authors concentrating on one velocity range without seriously considering that the gas in all three ranges may be intrinsically related. However, a link between IV and LV gas has been alluded to by Herbstmeier et al. (1995) and Albert & Danly (2004), who noted in their review of IV HI that such a relationship between the HV and IV gas is unclear and that the apparent connection in the sky between low-, intermediate- and high-velocity features is tantalizing. It will be shown below that this is far more than a tantalizing possibility.

The highly sensitive *WMAP* observations of weak, high-frequency (23 to 94 GHz) continuum emission over the whole sky are described by Hinshaw et al. (2006). They removed contributions from known sources of foreground galactic radio emission to produce the *ILC* all-sky map whose reduced angular resolution is also of order 0.6° . The *ILC* data (hereafter referred to generically as the *WMAP* data) for the Target Area were made available to the author in digital form as a function of rectangular galactic coordinates. The signal amplitudes for the Target Area range from -0.26 mK to +0.26 mK.

The *WMAP* team performed an extraordinary feat of correcting for all known sources of foreground radiation in order to obtain their final, *WMAP*, map. The structures that remained were then treated as having cosmological significance. However, it will be argued below that, instead, the *WMAP* (and *COBE*) workers may have uncovered evidence for one or more physical processes occurring in interstellar space that were not, and perhaps could not have been, predicted.

In essence, our study suggests that the *WMAP* map at $b \geq 30^\circ$, contains evidence for sources for weak continuum radiation originating at the interface between colliding HI clouds, or where moving HI structures interact with regions of enhanced interstellar plasma density.

Note that a direct comparison between the *WMAP* and earlier *COBE* data can be found at <http://map.gsfc.nasa.gov>. This comparison highlights the fact that the *WMAP* data represent a more sensitive, higher resolution version of the *COBE* results and thus any associations that may be identified between *WMAP ILC* structures and HI features has a direct bearing on the interpretation of the *COBE* results.

For the work reported here, HI maps were produced in rectangular galactic coordinates (l, b maps) to display the integrated HI brightness over a small velocity range. In the figures that follow the HI distribution is plotted using inverted gray-scale shading. Only a small fraction of the hundreds of $l-b$ maps that were produced during the present study will be shown to illustrate key points. In the overlays of continuum data onto the HI maps, the *WMAP* data are plotted as contours to indicate the extent of the positive continuum signals compared to the HI morphology. The choice of contour levels and these methods of display were determined by the need to make as clear as possible in published form the nature of the specific relationships that were found. A uniform vector offset between paired structures in search of a cross-correlation coefficient that would quantify such a relationship

over large areas of sky is unlikely to succeed because the observed offsets are not oriented in any systematic direction. Future cross-correlation studies should be confined to small areas around individual structures.

All of the areas where associations between *WMAP* continuum emission and HI structure were found, latitude-velocity (b, v) plots were also examined to determine how the various HI features to which the continuum data drew attention relate to one another. This led to the unexpected discovery of several properties of diffuse interstellar HI that cast light on the phenomenon that creates associations between the continuum and HI structures.

3. Comparison Statistics

The study began by comparing maps of the *WMAP* continuum emission and HI structure for the Target Area. The galactic HI sky is filled with small-scale structure evident in l, b maps (e.g., see Hartmann & Burton, 1997) so that any attempt to compare with small-scale structure found in the *WMAP* data, which also consists of multiple small peaks, will lead to chance agreements in position. Whether or not the associations between *WMAP* and HI peaks found in the Target Area are due to chance can be tested (to first-order) by overlaying the *WMAP* map for the Target Area data on the HI l, b maps for a Comparison Area, chosen as $l = 180^\circ$ to 300° , $b = 30^\circ$ to 70° , located symmetrically opposite the galactic anti-center with respect to the Target Area, and then again noting how many coincidences or close offsets are found. To this end, 25 l, b maps showing the integrated HI content over a 10 km/s range in 10 km/s steps between -250 & +50 km/s were produced for the Target Area. For the Comparison Area, 20 such maps from -120 to +80 km/s were produced to cover the extent of the galactic HI emission there.

Next, a list of the 33 brightest *WMAP* sources in the Target Area was generated and

the HI examined toward each of them to search for any associations between peaks. This number was chosen in order to include those associations that appeared to be the most interesting to initial visual comparison. The list could be enlarged in future. Continuum peaks within 1° of the boundaries of the Target Area were excluded in case the associated HI exists at or outside those boundaries. Table 1 lists the coincidences between HI and continuum peaks in the Target Area that were readily found in this analysis. An identifying number for the continuum source is given in column 1 and its galactic coordinates (in degrees) in columns 2 & 3. The peak *WMAP* brightness temperature in mK is given in column 4 while column 5 shows the number of adjacent HI maps separated by 10 km/s in which either an overlap in position or a closely offset association is found. Column 6 shows the velocity range of the putative associations and column 7 notes whether the association is aligned in position (on), offset by an angle of order 2° or less (offset), or both, due to spatial velocity gradients in the HI structure (marked both). Columns 8 & 9 list the Section numbers and Figure numbers used in the discussion below. Those entries marked with an x indicate the presence of very complex HI and related *WMAP* structure that will require more detailed study than is offered in this initial report to unequivocally identify associated features.

The virtual associations found by comparing the *WMAP* data for the Target Area with HI data for the Comparison Area are listed in Table 2. Columns 1, 2 & 3 are the same as for Table 1. Column 4 gives the true longitude for the Comparison Area HI and columns 5 through 8 correspond to columns 4 through 7 in Table 1.

Nine cases of overlapping features for the Target Area are listed in Table 1 which could be identified in at least 2 adjacent HI maps. Another two are obvious in only one l, b map. None are found in the Comparison Area in Table 2. Only one source in the Target Area (No. 12) shows no association with obvious HI structure in any of the 10 km/s wide bands

while 19 such cases are found in the Comparison Area. Together, these indicate that the claimed associations in the Target Area are unlikely to be due to chance.

An additional measure of whether or not the associations are real can be estimated by counting the number of maps in which associations are found for the Target Area versus the Comparison Area. For example, continuum source 1 is identified in 5 HI maps (each 10 km/s wide), thus it counts for 5 entries. The total associations noted in this way for the Target Area is 103. This compares with 21 in the Comparison Area and offers another estimate of the number of chance coincidences that might be expected in the Target Area.

A third method for estimating the likelihood of chance associations made use of a contour map showing the brightest 33 negative *WMAP* peaks and overlaying that on both the Target and Comparison Area HI l, b maps. For directions above $b=40^\circ$ no direct alignments were found for either Area, but for $b < 40^\circ$ two cases were found for both Areas. It was further noted that the number of close associations between the negative *WMAP* peaks and HI structure is a function of galactic latitude, which implies chance coincidences due to increased HI structure at lower latitudes. No such relationship was found for the key associations and close offsets for the Target Area.

4. On the Expected Number of Chance Associations

In the sections to follow it will be shown that, by taking a closer look at putative associations between ILC structure and HI features referred to above, previously unrecognized properties related to interstellar gas dynamics are revealed. This implies that the apparent associations between HI and *WMAP* structures are in fact real. It may be argued that despite the above general statements positional associations are due to chance and thus one should attach no weight to the fact that something new is learned by treating

the *WMAP* map peaks as guides to interesting areas of the local interstellar medium.

Here we will attempt to estimate in a more formal sense the number of chance associations to be expected when comparing two sets of data represented by the *WMAP* map and the HI maps. These attempts are necessarily limited by available data and a relative lack of pre-existing knowledge related to the statistics of small-scale HI emission structure that might have a bearing on this issue.

The morphologies of both HI and *WMAP* structures are complex yet distinct brightness features of a small angular extent of order 1° to 2° are common in both classes of data. Hence an order of magnitude estimate can be made of the likelihood of chance positional coincidences between peaks in the two types of structure, assuming both to be randomly distributed on the sky. This is a valid first approximation because if the ILC structures are indeed cosmological there should be no association with galactic structure whatsoever.

In the analysis described above the 33 brightest *WMAP* peaks ($= N_{Wpeaks}$) were identified in the *WMAP* (specifically the *ILC* map) covering an area, A , of 4,800 square degrees (see Table 1). The HI data were produced in the form of contour maps representing the integrated HI brightness over a 10 km/s band every 10 km/s from -200 to +50 km/s. Typically about 10 to 15 contour levels were plotted for each map and the number of peaks, defined as sets of closed contours with dimensions of order 1° to 2° , identified. The total, N_{Wpeaks} , is approximately 550 for the Target Area. However, a given HI peak on one contour map can usually be followed over at least two adjacent maps for HI at velocities outside ± 20 km/s with respect to the local-standard-of-rest; that is, over 3 adjacent velocity maps, which reduces N_{Hpeaks} by a factor of 3. In our study of HI features associated with *ILC* structure in the Target Area the relevant HI peaks could be followed over as many as 8 maps (i.e., 80 km/s). For low velocity HI ($-20 < v < 20$ km/s), narrow emission line components of order 6 km/s wide tend to appear less prominent in a contour

map integrating over a 10 km/s width. This detail is not at issue since the majority of the associations between *ILC* and HI peaks noted in the 10 km/s wide HI maps are not at low velocities.

The data summarized in Table 1 show that 33 *ILC* peaks are found to be associated with 103 HI structures in individual maps made at 10 km/s intervals, which also implies that on average each is found in 3 adjacent velocity maps. Hence the value of N_{Hpeaks} , is taken to be $550/3 = 183$. Using this number it is possible to estimate how many HI peaks (N) will lie within a distance r of any *ILC* peak; that is, within an area of order πr^2 square degrees centered on the *ILC* peak. This is given by

$$N = \pi r^2 A^{-1} N_{Wpeaks} N_{Hpeaks}. \quad (1)$$

The results of the estimates obtained using Eq.1 that follow are summarized in Table 3.

4.1. Directly Overlapping Associations

An overlap in position between two peaks is defined as having the centers located within 0.3° of one another (half the HI beamwidth), although in some of the examples discussed below the coincidence in position is $\leq 0.1^\circ$. Using $r = 0.2^\circ$, Eq. 1 predicts $N = 0.4$, which essentially means that no perfect overlaps in position are expected between the 33 *ILC* peaks and the 183 HI peaks. However, Table 1 shows that 9 (+2) coincidences of this order were found.

For the Comparison Area 20 maps covering a velocity range from -120 to +80 encompass the HI emission and approximately 280 peaks were identified. Using the condition that HI features are typically found in three adjacent velocity maps, $N_{Wpeaks} = 93$ for the Comparison Area. The number of direct associations due to chance is then $N = 0.1$. In this case, none were found, consistent with purely random coincidences in position.

This supports the conclusion that the overlapping pairs of *ILC* and HI peaks found in the Target Area are physically significant.

When HI column-density maps integrated over 2 km/s and plotted every 2 km/s are examined, more associations, especially at low velocities, emerge. No attempt has yet been made to quantify these relationships here and other workers are urged to give this challenge some attention.

4.2. Associated but Offset Peaks

Our analysis revealed that an *ILC* peak is often located close to but slightly offset from an HI structure with a similar morphology, again with dimensions of order 1° to 2° . A formal estimate of the likelihood of finding morphologically similar structures in the HI and ILC maps apparently located adjacent to one another is not readily calculated. However, following the approach used in §4.1 it is possible to obtain an approximation.

In the Target Area the offset between similar structures found by comparing the *ILC* and the 25 different HI maps are usually of order 1.0° from the HI peak (see Figs. 3, 4, 7 8 & 9). Eq. 1 can thus be used to determine the number of cases where the center of an HI feature may be expected to lie within 1.0° of an ILC peak due to chance alone. For the Target Area this is 5.1, which compares to the 11 cases where the HI feature can be followed through at least 2 adjacent velocity maps. This constraint highlights the fact that our estimate of chance associations marked by a small offset is, at best, a rough calculation because there are many complexities acting to make the task more difficult. For example, what physical phenomenon could be invoked that would produce precisely the same morphology in both the *ILC* map and an associated HI feature at some velocity? As will be mentioned in the discussion, the continuum emission appears to be produced where

HI in interacting with other HI or with plasma and there is no *a priori* reason to expect this interaction to be nicely uniform because localized volume densities of HI or plasma will play a role in defining the shape of the observed structure.

The average separation for the four paired structures in the Comparison Area (Table 2) is approximately 1.5° , which means that $N = 5.9$ such pairs are predicted by chance, consistent with the five that were found in 2 or more adjacent velocity maps. In only one of these examples (No. 16 in Table 2) could the structure be followed over more than 2 adjacent velocity maps whereas in the Target Area some offset pairs could be followed through as many as 5 adjacent maps.

4.3. Limits to these Estimates

These estimates are limited for several reasons. One is that we treat the two classes of structures as being random on the sky, which is not so for HI, because it is highly filamentary. Also, no account is taken of morphological similarities other than sets of closed contours on a scale of 1° to 2° . Morphological similarities are difficult to quantify in a formal manner but in any event would reduce the likelihood of chance associations. For example, in the case of the overlapping structures illustrated in Fig. 6 below, two elongated HI features, one showing a strong velocity gradient, overlies an elongated ILC feature with the major axes of all three agreeing to within 5° , highly unlikely if due to chance.

Another limitation to refining the above calculations concerns the nature of interstellar HI structure itself. At low velocities, HI emission profiles show narrow components that can vary dramatically over small angles on the sky. Such spatial differences on scales of less than 1° between area maps made at 2 km/s intervals are well known whereas at intermediate and high velocities the underlying profiles are inherently broader and a given peak (cloud)

may be identified over a large velocity range, as much as 30 km/s or more.

It is beyond the thrust of this paper to enter into a detailed discussion of these issues. Suffice it to say, this brings us back to the underlying fact that if the *WMAP* small-scale structure is cosmological in origin then there should be no cases whatsoever of dramatic associations with galactic HI structure.

These rough estimates suggest that the coincidence in position or small offsets between HI and *ILC* peaks in the Target Area reveal the presence of a previously unrecognized source of weak continuum radiation arising from physical processes occurring at the surface of HI features (clouds) or filaments interacting over some fraction of their lengths. It will be demonstrated below that closer examination of some of these putative associations reveals new properties of interstellar HI structure. In fact, the *ILC* data can be used to point to the existence of subtle physical phenomena related to galactic HI.

5. Case Studies of Associated HI and Continuum Structures

All of the entries listed in Table 1 were examined in detail using HI l,b maps made at smaller velocity intervals (2 and/or 5 km/s) and compared with the continuum emission structure. In the course of this closer examination, the l,b maps invariably revealed further coincidences in position not included in Table 1. With a few notable exceptions, these are not discussed further in this brief report. Most surprisingly, this analysis often led to the discovery of new aspects of interstellar HI structure, or it highlighted claims found in the literature that had been largely overlooked until now. The apparent associations in the Comparison Area listed in Table 1 were also examined more closely but revealed nothing of note other than might be expected from chance associations.

The individual cases of associated HI and *WMAP* features illustrated here were chosen

to highlight key points revealed by the most obvious associations. Discussion of those sources listed in Table 1 that are located in very complex continuum or HI structure will be deferred because that requires an extensive presentation of HI l, b maps at many velocities. By limiting this report to the most informative and relatively simple examples we adhere to the principle that to learn as much as possible about a new phenomenon it is better to consider the most clearly defined and simplest cases rather than risk becoming immediately immersed in too much information that is difficult to untangle.

The choice of data presentation in the next subsections was determined after examination of several hundred maps of the HI distribution in comparison with the continuum maps for the brightest *WMAP* peaks in the Target Area. Also, inverted gray-scale representations of the HI emission are overlain on contour plots of the *ILC* data because overlaying two sets of contour maps is too confusing to recognize out the crucial similarities we wish to point out in a plot that does not use color.

5.1. Source 24 at $(l, b) = (112.^\circ 3, 57^\circ.8)$: Directly overlapping HI and continuum features

Figure 1 (a) shows the HI brightness centered at -118 km/s integrated over 5 km/s (peak value 51 K.km/s). Fig. 1 (b) shows the HI brightness centered at -87 km/s integrated over 5 km/s (peak value 47 K.km/s). By using Gaussian analysis of the HV and IV gas every $0.^\circ 5$ in latitude or longitude across the peaks, the coordinates of the centers of the HI structures were derived and found to be identical in latitude ($b < 0.^\circ 1$) and also identical to the latitude center of the continuum structure. The center of two HI features are also identical in longitude but offset from the continuum peak by $0.^\circ 3$, half the beamwidth used in the HI studies.

Examination of the latitude-velocity (b,v) plot at $l = 112^\circ$ revealed no significant HI emission at -100 km/s between the two features seen in (a) and (b). However, a marked lack of LV emission around zero velocity is revealed. Fig. 1 (c) shows the integrated HI content over the velocity interval -8 to +2 km/s with the continuum contours overlain. The peak in the continuum emission is clearly co-located with a lack of low-velocity HI. Also at low velocities an HI peak at $(l,b) = (115^\circ, 57^\circ)$ is located at the same position as a secondary peak in the continuum emission. Further relationships emerge when the integrated HI emission between -130 & -120 km/s is examined, Fig. 1 (d). In addition, two maximum at $(l,b) = (113^\circ, 55^\circ)$ and $(l,b) = (115^\circ, 54^\circ)$ are evident and overlie HI minima seen in (c).

These plots show a direct relationship between HV & IV gas and a distinct minimum in LV HI, with all of these related to the presence of a *WMAP* continuum emission feature. The possibility that small-scale IV HI structure is associated with a lack of LV gas, has been noted by Burton et al. (1992) as well as Kuntz & Danly (1996). Here we find striking confirmation, something that would not have been noticed but for the presence of a significant peak in the *WMAP* continuum emission data that drew attention to this specific area of the sky.

5.2. Sources 1 & 5 at $(l,b) = (140^\circ, 40^\circ)$: Interacting filaments, part 1

Two of the brightest continuum emission peaks listed in Table 1 are a pair found at $(l,b) = (140^\circ, 40^\circ)$. Figure 2 shows the relationship between continuum emission and HI brightness integrated over the four velocities intervals indicated. The HI peaks correspond to values of 126, 143, 63 & 61 K.km/s for the four frames respectively. In all four of these plots, filaments of HI pass through the location of the overlain double continuum emission peak. Furthermore, the continuum peaks are located in regions of localized minimum emission within each filamentary feature. It appears as if the filaments are focused on, or

originate in, the continuum feature. These HI filaments form part of a larger arc of HI emission sometimes referred to as the North Celestial Pole loop, which has been extensively studied in regard to its molecular and dust content (Pound & Goodman, 1997). We cannot offer an extensive review of such data but do note that a full understanding of this area will require that the HI mapping be done at 1 km/s intervals in order to determine what mechanism may underlie the remarkable association between overlapping, and in all likelihood interacting, HI filaments and the double continuum source.

5.3. Sources 11 & 30 centered at $(l,b) = (119.^\circ5, 57^\circ)$: Association between HV and LV HI

Figure 3a shows the HI structure of HV gas integrated between -140 and -110 km/s associated with two *WMAP* continuum sources, 11 & 30 identified in (b). They are linked by a ridge of emission straddled by two HI features (peaks 22 K.km/s) whose morphologies closely follow the continuum radiation contour lines. Gaussian analysis of the HI profiles in a $0.^\circ5$ grid for the entire area covered in Fig. 3a was carried out and allowed the center velocities of the two HI components to be determined. They are -127 and -118 km/s for the northern and southern peaks, respectively. The Gaussian analysis also allowed the HI column density for two other features to be mapped, shown in (b) and (c). Their presence was recognized in a set of HI emission profiles at $l=120^\circ$ shown in Fig. 3d. Most striking is a component at -8 km/s, seen only at $(l,b) = (120^\circ, 57^\circ)$. It has a peak column density of $7 \times 10^{18} \text{ cm}^{-2}$ and its morphology is plotted in Fig 3b, which shows that it is located precisely on the saddle in the continuum contours between two peaks. Even more striking is the fact that it is unresolved in latitude while slightly elongated in longitude along the continuum ridge axis.

Fig. 3(c) shows the column density plot for the -17 km/s feature seen in (d), again

based on the results of the Gaussian analysis of the area profiles (peak column density $19 \times 10^{18} \text{ cm}^{-2}$). The location of this component is also related to the presence of the continuum ridge with the southern peak located at the position of the HV peak that nestles in the indentation (or pinch) in the continuum emission ridge. At this stage of the analysis, no clear relationship between intermediate velocity HI structure and other features in the area of Fig. 3 has been noted. However, weak positive velocity HI emission is also found toward this structure and it will require confirming observations to determine its nature.

The data in Fig. 3 represent an example of a close relationship between HI structures at low and high velocities, with each of them related to the presence of continuum emission, a relationship that emerged because attention was drawn to this area by the presence of the peaks in the *WMAP* continuum emission data.

5.4. Sources 19, 32 & 33 in an area centered at $(l,b) = (93^\circ, 37^\circ)$

This is the first of several highly complex areas identified in the Target Area as regards the distribution of both the continuum and HI structure but which nevertheless show an underlying order. A closer look led to further insights into the nature of the associations that form the thrust of this report.

5.4.1. Overview of sources 19, 32 & 33

Figure 4 shows six views of the HI structure at the velocities indicated with the continuum contours overlain. In (a) the HI structure is integrated from -180 to -170 km/s (peak value 9.5 K.km/s) and two vectors are added to the plot to represent the optical polarization position angle for two stars, HD151101 at a distance of 96 pc at $(l,b) = (95.^\circ 67, 38.^\circ 16)$, PA = 141°, and HD155761 at a distance of 81 pc at $(l,b) = (96.^\circ 01, 35.^\circ 04)$, PA

136°. [These position angle data are from the summary list of Heiles (2000)]. These vectors lie parallel to the axis that joins the three continuum sources 32, 19 & 33, which is found to have a position angle of 132° and, in turn, all are oriented parallel to the axis of Loop III as determined by inspection of the low frequency mapping by Berkhuijsen (1971). The ridge-line of Loop III is just off the eastern edge of Fig. 4. According to Spoelstra (1972), Loop III represents the emission from an old supernova shell at a distance of order 150 pc. In Fig. 4a, a set of HI peaks is associated with and slightly offset from each of the continuum peaks with a ridge of HI bridging the space between source 33 and the peak at the north end of the area. The HI at the location of source 32 is directly associated with *WMAP* structure and its morphology will be discussed in the next section.

Fig. 4b shows the same continuum contours as in (a) overlain on the HI brightness integrated over a 2 km/s interval centered at -150 km/s (peak value 12.6 K.km/s). Figs. 4 (c), (d) (e) & (f) show the continuum contours overlain on the HI brightness temperature at the velocities indicated (peak values 3.7, 8.3, 9.7 & 9.1 K.km/s respectively). In each case the HI peaks straddle the continuum emission peaks. The maximum HI emission in a 2 km/s wide band at -150 km/s is closely associated with but offset from continuum source 19 by about 2°. This order of offset between the peaks is found to be common for many of the sources listed in Table 1 and implies that the underlying mechanism is localized to the boundaries of the HI features, whose diameters are also of this order.

5.4.2. *Continuum source 32 at $(l,b) = (89.3^\circ, 34.5^\circ)$ and associated high-velocity HI*

Figure 5 illustrates the dramatic association between *WMAP* emission peak 32 and HI. Here nine inverted gray-scale images of the HI are overlain by a contour map of the continuum brightness. All the plots are single channel maps (1 km/s wide) and the peak brightness temperatures are all of order 0.8 K, except for the map at -200 km/s where the

peak is 0.3 K and at -150 km/s where it is 1.1 K. The limits of the associated HI emission are -135 km/s at the same location as the peak at -140 km/s, and -205 km/s. The HI centroid of emission shifts in velocity as it follows the ridge of the *WMAP* emission feature. The plots in Fig. 5 show a bifurcation of the HI peak starting at -170 km/s with each of two components shifting along opposite sides of the continuum ridge as the velocity is increased.

A preliminary attempt to sketch the structure revealed in these and HI l, b maps at smaller velocity intervals suggests a twisted pattern around an axis defined by the continuum radiation, possibly related to magnetic field structure, although we have been unable to picture a simple three-dimensional description of what might be happening around this axis. Higher resolution HI data are desirable to untangle the HI structure in this fascinating area. These plots offer dramatic proof that the HI and continuum emission for this area are directly related.

5.4.3. *Continuum source 32 and associated intermediate- and low-velocity HI*

Examination of b, v plots and emission profile data for this area revealed further details that are relevant to understanding the relationship between the HI and continuum structures. This is illustrated in Fig. 6a in which several HI emission profiles cutting across the continuum feature seen in Fig. 5 are shown. In a manner similar to that reported in §5.3 above, a distinct additional component, in this case at -40 km/s, emerges in one of the profiles. Its morphology is shown in Fig. 6b as an inverted gray scale image (peak value 6.7 K.km/s for the -42 to -38 km/s map) with the same continuum emission contours shown in Fig. 5 overlain. This HI component is clearly associated with the continuum and the HI structure at high velocities seen in Fig. 5. Fig. 6c illustrates in contour map form how closely this IV HI structure (contours from 3 K.km/s in steps of 0.05 K.km/s) mimics the continuum contours seen in (b).

Further examination of the b,v contour maps reveals a phenomenon also found for the HI-continuum association noted in §5.1 above, which is a dearth of low-velocity emission where the anomalous velocity HI structure shows a peak. This is illustrated in Fig 6d where the integrated HI emission from 5 to +15 km/s (peak 36 K.km/s) is shown. A distinct minimum (36 K/km/s, compared to the maximum value in this plot of 112 K.km/s) in the low velocity integrated HI emission is found at the location of the peak in the IV HI emission at -40 km/s, and, in turn, this coincides with the location of continuum source 32 and the HV structure seen in Fig. 5.

5.5. Sources 3, 9, 18 & 33 in an area centered at $(l,b) = (140^\circ, 65^\circ)$

A dramatic case of multiple associations between HI and continuum emission structures is found in the area illustrated in Figure 7a. A long corkscrew-like HI filamentary feature (here integrated from -100 to -90 km/s) extends from $(l,b) = (120^\circ, 60^\circ)$ to $175^\circ, 67^\circ$ in this velocity interval and can be followed in a wide arc to $(l,b) = (80^\circ, 30^\circ)$ in the Target Area. It is very evident in the maps shown by Hartmann & Burton (1997). The HI in the whole area at $l > 140^\circ$ is known as Complex M; see for example, Herbstmeier et al. (1995). The same gray-scale image plotted in Fig. 7a is repeated in Fig 7b with the *WMAP* continuum data overlain. Clearly both types of emission are complex over the area yet a considerable degree of order can be recognized. For example, a ridge of continuum emission across the center of the map between $(l,b) = (138^\circ, 67^\circ)$ and $(l,b) = (146^\circ, 66^\circ)$ has a low brightness counterpart in the HI emission along $b = 66^\circ$. Also, a small, weak arc of emission at the top center of the map in Fig. 7b is present in the HI and slightly offset to the south of the continuum.

Every continuum peak in the area of Fig. 7b exhibits an associated and usually slightly offset HI feature at some velocity in the range -140 km/s to +20 km/s. This is highlighted

in the detailed view in Fig. 7c where an the continuum feature from $l=138^\circ$ to 146° bridges the gap between the HI peaks at the center and right, and other continuum contours encircle the HI peaks at the center and left side of the map. The continuum structure illustrated here does not contain any of the brighter *WMAP* sources listed in Table 1 but it does serve to illustrate that further significant associations between HI and continuum structures emerge from a closer look at HI data. Fig. 7c shows that the two types of emission are morphologically similar in that a shift of about 2° of the HI to the northeast creates a high degree of correlation with the continuum structure. We tested this assertion numerically by performing a limited cross-correlation analysis and the result revealed no more than can be seen in Fig. 7c. This offset relationship again suggests that the continuum emission is being produced at the surface of HI structures interacting with their surroundings. When the motion of the HI is along the line of sight the HI and continuum emission will be aligned but more generally the motion will have a component across the line of sight and HI and continuum emission will then appear offset on the sky.

Continuum source 3 at $(l,b) = (160.^\circ3,62.^\circ9)$ as labeled in Fig. 7b exhibits associated HI features at a number of velocities and deserves a separate report.

5.5.1. Close-up view of source 18 (HVC MI)

Figure 8 is a detailed view of a section of Fig. 7 to illustrate a clear association between HI and continuum emission. This inverted gray-scale image shows the HI brightness integrated over the velocity range -140 to -110 km/s is offset from and parallel to a pair of continuum emission peaks, source 18 (integrated brightness 100 K.km/s) and a companion. This double HI feature is well known and corresponds to high-velocity cloud HVC MI, which forms part of the extension to the corkscrew-like feature shown in Fig. 7. The angular separations between the peaks in the HI and *WMAP* continuum structures in Fig.

8 are $2.^{\circ}8$ in HI and $3.^{\circ}0$ for the continuum. The offsets between these paired peaks is $1.^{\circ}6$ for the northern pair and $1.^{\circ}3$ for the southern pair.

A crucial clue as to the likely cause for associations between the small-scale HI and high-frequency continuum structure is found in a report of excess soft X-ray emission toward HVC MI found by Herbstmeier et al. (1995). Their Figure 7a has been adapted to correspond to the data in Figs. 8a & b above and it is shown as Fig. 8c. The contours correspond to the HI emission from HVC MI, similar to the data in (a) and the shaded pixels overlain correspond to excess soft x-ray emission. Similarly, Tufte, Reynolds & Haffner (1998) have reported excess $H\alpha$ emission at several positions toward HVC MI. No doubt the close spatial relationship seen in Fig. 8c between the X-ray hot spot and the HI and the high-frequency continuum emission observed by *WMAP* as well as the presence of $H\alpha$ emission contains critical clues that should lead to understanding the nature of the associations between HI and weak, high-frequency continuum emission.

In Fig. 8d the *WMAP* contours are overlain on the LV HI data. Again a relative lack of LV emission, here integrated between 5 & $+5$ km/s, is seen to be closely associated with the continuum and HI structure at high velocities. The HI column density is 1.8 K.km/s for the minimum compared to 6.2 K.km/s for the maximum at the top left of (d)

Based on what is seen for HVC MI it is predicted that its companion, known as HVC MII, located at $(l,b) = (185^{\circ}, 65^{\circ})$ beyond the boundaries of the Target Area, will also exhibit a close association with continuum emission structure.

[Following the initial submission of this report in November 2006, the author was sent *ILC* data for two strips of sky covering all longitudes for northern and southern latitudes between 30° & 70° . These data were received Dec. 2, 2006 (with thanks to Gary Hinshaw and Wayne Landsman). This represents an additional 5 times as much data as encompassed in the Target Area and many positional associations and close offsets were quickly found

in the other areas of sky. This will be described in a subsequent paper. However, the availability of these data offered an immediate opportunity to test the prediction made above, that HI and *ILC* data toward HVC MII at $l, b = (183^\circ, 65^\circ)$ from $v = 80$ to 60 km/s would show an association. This is precisely what was found. Toward HIV MII, the *ILC* contours encompass three-quarters of the circumference of the HI peak while excess soft X-ray radiation observed by Herbstmeier et al. (1995) and $H\alpha$ emission reported by Tufte, Reynolds & Haffner (1998) are also associated. The details of this will be also be described in a subsequent paper.]

5.6. Sources 15, 16, 17, & 29 in an area centered at $(l, b) = (85^\circ, 60^\circ)$

The area shown in Figure 9 shows considerable complexity in both the HI and continuum emission. This is difficult to untangle although examination of the data does lead to the discovery of informative associations between HI and continuum structures not listed in Table 1.

5.6.1. HI and continuum around $(l, b) = (88^\circ, 58^\circ)$: Interacting HI filaments, part 2

Figure 9 shows the HI brightness at the four velocities indicated and the continuum emission contours are overlain. In Fig. 9a the inverted gray-scale image of HI brightness at -44 km/s reveals a long curving filament extending from $(l, b) = (100^\circ, 70^\circ)$ down to $(l, b) = (78^\circ, 50^\circ)$. It avoids the complex of continuum emission centered at $(l, b) = (75^\circ, 57^\circ)$, which contains sources 16 and 17 labeled in Fig. 9b. That complex is associated with an equally complex set of HI filaments spread over a range of velocities that will not be considered here. Instead, we draw attention to the structure at $(l, b) = (88^\circ, 58^\circ)$ near the center of the map. There the HI in the filament seen at -44 km/s, which can be traced in contour maps

to 36 km/s over much of its length, manifests two bright peaks on its axis. These are found precisely where a low-velocity filament, shown in the Fig 9d for HI between +6 and 0 km/s, terminates at and intersects with the intermediate velocity filament seen in (a). It is also evident in Figs. (a), (b) & (c) that with changing velocity the orientation of the pair of HI peaks rotates about the continuum source between them.

5.6.2. Pairs of HI features and continuum sources

Figure 10 offers details regarding the association between HI and continuum emission for two pairs of HI features. Fig. 10a shows the pair at $(l,b) = (88^\circ, 58^\circ)$ referred to in §5.6.1 where the continuum source is located on the axis of the double HI feature and bridges the gap. A similar closely-spaced pair of HI peaks located to either side of a continuum peak is found at $(l,b) = (92^\circ, 62^\circ)$, shown in Fig. 10b. This pair is also found on the axis of the -44 km/s HI filament at a location where another HI structure, observed at velocities between -12 to -18 km/s, intersects the former.

5.7. Source 21 at $(l,b) = (135.^\circ 1, 51.^\circ 1)$: another clear case of overlapping structures

Figure 11 shows the HI structure in the 6 velocity regimes indicated. In the first three frames the HI emission is relatively weak but between -49 & -39 km/s it is very bright. At those velocities, *WMAP* source 21 and the HI are perfectly coincident in position but in frames (a) and (b) the (weaker) related HI peak is shifted slightly to the west.

The perfect alignment in position of the continuum and HI peaks seen in frames (c) through (e) is reminiscent of the aligned sources found in §5.1, Fig. 1 & §5.4.2, Fig. 5. In both those cases a significant lack of low-velocity HI was also noted to be coincident in

position with the HI and continuum peaks. The same is found here, as is illustrated in Fig. 11f. The bulk of the continuum emission around source 21 lies in a distinct local minimum in the HI brightness. The deepest hole in the HI lies at the southern tip of continuum source 21 and the general absence of low-velocity gas seen in Fig. 11f clearly encompasses the overlying HI. This area, like so many of the more complex ones referred to above, is deserving of a closer look.

6. Discussion

The goal of this study was to determine if any evidence exists to suggest that small-scale structure in the *WMAP* data and HI are related. To that end, the continuum emission data guided the study and surprisingly led not only to the discovery of what appear to be highly significant relationships between the two data sets but also drew attention to unexpected properties of the galactic HI that turned out to be uniquely interesting.

In general, high latitude continuum emission peaks found by *WMAP* in a Target Area ($30^\circ \leq l \leq 70^\circ$, $180^\circ \geq b \geq 60^\circ$) have a corresponding HI peak at the same location or slightly offset by 1° to 2° in position that is found in two or more l, b maps made at 10 km/s intervals. Angular offsets of the same order between parallel HI, dust and $H\alpha$ filaments have been reported by Verschuur et al. (1992). In several of the cases shown above the HV or IV structures are clearly related to local minima in the LV structure at the same position (see §5.1, §5.4, & §5.5). This confirms the suspicion noted by Burton et al. (1996) and Kuntz & Danly (1996) that IV HI structure is sometimes directly associated with an absence of low velocity HI emission on a small scale. This can be taken a step further by noting that the anomalous velocity HI at both high- and intermediate-velocities is in several cases associated with a lack of low-velocity emission but in some examples a low velocity peak at a different velocity from the minimum may be associated with anomalous velocity

HI (see §5.3, §5.4, & §5.5).

In §5.2 & §5.6.1 it was suggested that in some cases *WMAP* sources are located where HI filaments are interacting. The filaments in question are seen largely normal to the line-of-sight, otherwise they would not produce such striking elongated patterns on the sky. In these cases, a lack of HI emission at the location of the continuum peaks is clear since the continuum peaks lie between pairs of peaks in the HI emission.

6.1. A Model

It is unlikely that a single physical process or phenomenon can account for the range of examples given above, although it is likely that the geometry describing the relative motion of the HI gas mass relative to another structure or through interstellar space will account for occasional perfect alignments or the more frequent small offsets seen in the data (Table 1). The common denominator that underlies all the associations discussed here is that the *WMAP* peaks are associated with HI features where two HI structures may be interacting (probably colliding). This is based on often finding evidence for two features at distinctly different velocities coincident in position at the location of the *WMAP* feature. In other cases two HI features at (nearly) the same velocity straddle a continuum emission peak in position, for example as shown in Fig. 10.

Depending on the geometry of the situation, positional coincidence will be observed in directions where a collision between two HI features (clouds) occurs along the line-of-sight. However, when the HI features are interacting while moving along an axis oriented at some angle to the line-of-sight the relationship will be observed as closely offset structures.

A number of clues that may help account for the physics underlying the production of continuum emission at the surface of moving HI structures exist in the literature. For

example, as was described in §5.5.1, Herbstmeier et al. (1995) report excess soft X-ray emission at the boundary of HVC MI where the *WMAP* continuum structure is prominent (Fig 8). On a larger scale, Kerp et al. (1999) find evidence for widespread soft X-ray emission over much of our Target Area toward the HV structures but the angular resolution of their data do not allow for closer comparison with our results. Furthermore, $H\alpha$ emission has also been found toward HVC MI, HVC MII and other high-velocity features, Tufte et al. (1998). This raises tantalizing questions as to the emission mechanism that could produce the continuum radiation. Perhaps it involves the formation of dust at the (shocked) interface between the HI and surroundings by a mechanism involving spinning dust grains such as has been proposed by Draine & Lazarian (1998). However, we might expect that at best very small quantities of dust will be created at the interface between colliding, diffuse HI features.

Another interesting phenomenon that may have a bearing here is found in Liu & Zhang (2006) who studied the cross-correlation between *WMAP* and Egret γ ray data and concluded that an unknown source of radiation, most likely of galactic origin, was implied by their analysis. That would produce foreground residuals that should be removed in order to minimize their role in confusing the cosmological interpretation of the *WMAP* data. It now seems likely that the source of this unknown radiation of galactic origin may be found in processes occurring at the surface of HI structures moving through interstellar space or interacting with one another, as illustrated in §5. A possible mechanism for producing the seed electrons at the surface of moving HI features which then give rise to continuum radiation is suggested by Verschuur (2007) but further consideration of that model is beyond the scope of this report.

It is hoped that research into the relationships between interstellar HI morphology and high-frequency continuum radio emission observed by *WMAP* will be stimulated by the

above discussions.

7. A Note on the Angular Power Spectrum of the HI Structure

The angular power spectrum of the *ILC* structure (e.g., Fig. 16 of Hinshaw et al., 2006) is widely regarded as strong confirmation of the cosmological origin of the *ILC* (*WMAP*) structure. Given that we are claiming that the *ILC* structure has a galactic origin, and that it is associated with interstellar HI features, the question arises as to whether the angular power spectrum of galactic HI structure is responsible for producing the shape of the cosmological angular power spectrum. No one has attempted to derive a similar spectrum for galactic HI structure because there would have been no reason to do so. Perhaps those with the necessary tools will undertake the challenge, which will be awesomely difficult, given the complex nature of HI structure at high galactic latitudes that extends over a velocity range from 250 to +200 km/s with respect to the l.s.r., and given that the HI structure may be quite different even in 2 km/s intervals in the low-velocity gas. Any such attempt will surely have to be limited to high galactic latitudes to avoid the complexity of HI in the galactic disk, which it will be impossible to untangle due to velocity crowding.

Our initial attempts to tackle this problem (inspired by a suggestion made by Shuang-Nan Zhang and Richard Lieu, private communication) show that on any scale over which the *ILC* data might be averaged in latitude or longitude (for example over 40° in latitude or 90° in longitude in the Target Area, the resulting profiles of average brightness versus the other coordinate (longitude or latitude, respectively) manifest a series of peaks that each finds a counterpart in HI emission profiles integrated over the same spatial extent. In the preliminary tests performed to date it is possible to identify excess in HI emission over some velocity interval that matches each *WMAP* peak. The point is that the task of comparing the *WMAP* angular power spectrum with HI structure will be heavily

dependent upon taking into account all the HI structure at all velocities, bearing in mind a model that explains the claimed associations in terms of interactions between HI features (clouds) to produce the weak continuum emission detected by *WMAP* (and *COBE*). Not only must HI emission at all velocities be considered in such a study, but there is no *a priori* reason to expect that a uniform peak HI brightness (or integrated brightness) will be involved in any given association with an ILC peak.

8. Conclusions

In a Target Area (4,800 square degrees in extent), clear associations between foreground galactic HI features and structure observed by *WMAP* have been found. The latter structures are believed to have a cosmological origin and therefore should show no relationship to galactic foreground structure other than purely chance alignment in position. In a Comparison Area nothing like the associations found in the Target Area were recognized in the data. When the Target Area candidates for associated HI and continuum emission structures were examined in detail, a small offset of order 1° to 2° is often found between them. This suggests that physical processes at the surface of dynamic HI structures are producing enhanced continuum radiation. Where this interaction is viewed along the direction in which the HI is moving the continuum structure is observed to be overlapping in position but where the HI has a transverse component of motion the two forms of emission are seen offset on the sky.

Taken as an ensemble, these direct spatial associations and close offset between HI and *WMAP* emission peaks points to the existence of one or more processes occurring in interstellar space capable of generating weak, high-frequency continuum radiation. However, since the Target Area is marked by the presence of highly disturbed HI it may not be typical of other directions on the sky. [A preliminary look at the additional *ILC* data

obtained since the first version of this report indicates that the phenomenon is not limited to the Target Area.]

Those who favor a cosmological interpretation of the *WMAP* structures should consider the possibility that a previously unknown source of continuum emission in the Galaxy is playing a role in creating structure in the *WMAP* (and *COBE*) data. If, as a result of further studies along the lines described in this report, the associations discussed here are found to be common it would raise the specter that the microwave background emission has less small-scale structure than is now believed to be the case.

I am grateful to Wayne Landsman of the *WMAP* team who supplied the author with the *ILC* continuum emission data for the Target Area in digital form and in rectangular coordinates, and to Gray Hinshaw who encouraged this data transfer. I am particularly grateful to Tom Dame for providing me with the data cube of the LAB survey and the necessary software for a Mac computer to allow the production of the vast majority of the final area maps of HI emission presented in this paper. Without his software I could not have prepared the HI maps presented above in a finite time. I also greatly appreciate encouragement from and discussions with Joan Schmelz and Butler Burton as I formulated for publication this highly controversial report. In this context, the remarks by a referee are deeply appreciated. I also appreciate the important feedback offered by Dave Hogg, Mort Roberts, Ed Fomalont, Eric Priest, Piet Marten, Tony Peratt, Max Bonamente, Richard Lieu & Shuang-Nan Zhang.

REFERENCES

- Albert, C. E. & Danly, L. 2004, p. 73, High-Velocity Clouds, ed. van Woerden, H, Wakker, B.P., Schwarz, U. J. & de Boer, K.S. (Kluwer Academic Publishers: Dordrecht)
- Berkhuijsen, E., 1971, A&A, 14, 259
- Blaauw, A. & Tolbert, C.R. 1966, Bull. Astr. Inst. Neth., 18, 405
- Burton, W.B., Hartmann, D. & West, S.R.D., 1996, Unsolved Problems of the Milky Way, Eds. Blitz, L. & Teuben, P. (Springer: New York)
- Burton, W.B., Bania, T.M., Hartmann, D., & Yuan, T., 1992, "Evolution of Interstellar Matter and Dynamics of Galaxies", p25, Eds. Palous, J., Burton, W.B. & Lindblad, P.O. (Cambridge University Press: Cambridge)
- Drained, B.T. & Lazarian, A. 1998, ApJ, 494, L19
- Fejes, I. & Wesselius, P.R. 1973, A&A, 24, 1
- Hartmann, D. & Burton, W.B., 1997 Atlas of Galactic Neutral Hydrogen, Cambridge Univ. Press,
- Heiles, C., 2000, ApJ, 119,923
- Herbstmeier, U., Mebold, U., Snowden, S.L., Hartmann,D., Burton, W.B., Moritz, P., Kalberla, P.M.W., & Egger, R. 1995, A&A, 298, 606
- Hinshaw, G. et al. 2006. Available in electronic form at <http://lambda.gsfc.nasa.gov>.
- Kalberla, P.M.W., Burton, W.B., Hartmann, D., Arnal, E.M., Bajaja, E., Morras, R., & Pöppel, W.G.L. 2005, A&A, 440, 775
- Kerp, J., Lesch, H., & Mack, K.-H. A&A, 286, L13

Kuntz, K.D., & Danly, L. 1996, ApJ, 457, 701

Pound, M.W., & Goodman, A.A. 1997, ApJ, 482, 334

Tufte, S.L., Reynolds, R.J., & Haffner, L.M. 1998, ApJ, 504, 773

Spoelstra, T. A. Th., 1972, A&A, 21,61

Verschuur, G. L. 2007, IEEE Trans Plasma Sc., August, in press

Verschuur, G.L., Rickard, L. J., Verter, F., Pound, M.W., & Leisawitz, D., 1992, ApJ, 390,
514

Wakker, B.P., 2004, High Velocity Clouds, Eds.van Woerden, H., Wakker, B.P., Schwarz,
U.J., & de Boer, K.S., 25 (Kluwer: Dordrecht)

Table 1. TARGET AREA ASSOCIATIONS

No.	l	b	Temp.(mK)	No. Maps	Vel. (km/s)	Offset or On	Section	Figure
(1)	(2)	(3)	(4)	(5)	(6)	(7)	(8)	(9)
1	139.6	40.1	0.227	5	-60 to -50	both	5.2	2
1	-40 to -30	(see
1	10 to 20	text)
2	174.4	56.8	0.223	3	-120 to -90	offset	x	x
3	160.3	62.9	0.218	4	-130 to -110	offset	5.5	7
3	-30 to -10	offset
4	176.1	53.0	0.212	1	-20 to -10	offset	x	x
5	140.3	41.5	0.202	5	-60 to -50	both	5.2	2
5	-40 to -30	(see
5	-10 to 20	text)
6	172.3	59.5	0.199	2	-70 to -50	offset	x	x
7	174.0	50.5	0.182	2	-130 to -120	offset	x	x
7	-20 to -10	offset
8	177.2	57.6	0.182	1	-110 to -100	offset	x	x
9	168.1	67.4	0.180	6	-130 to -100	offset	5.5	7
9	-60 to -40	offset
9	-30 to -20	offset
10	171.6	56.3	0.179	4	-70 to -50	offset	x	x
10	0 to 20	offset
11	118.1	57.0	0.175	3	-140 to -110	offset	5.3	3

Table 1—Continued

No.	l	b	Temp.(mK)	No. Maps	Vel. (km/s)	Offset or On	Section	Figure
12	159.6	50.0	0.172	none	none	none	x	x
13	169.5	46.5	0.172	1	-20 to -10	offset	x	x
14	174.7	48.2	0.172	1	-20 to -10	offset	x	x
15	101.8	59.5	0.169	1	-10 to 0	offset	5.6	9
16	78.4	55.9	0.168	4	-30 to 10	both	5.6	9
17	82.3	55.7	0.168	2	-20 to 0	both	5.6	9
18	165.7	64.8	0.168	6	-140 to -90	offset	5.5	7,8
18	-20 to -10	on
19	91.5	36.7	0.166	9	-190 to -120	both	5.4	4
19	-40 to -30	(see
19	-20 to -10	text)
20	170.2	54.5	0.165	3	-60 to -50	offset	x	x
20	0 to 20	offset
21	135.4	51.1	0.164	1	-50 to -40	on	5.7	11
22	151.2	48.8	0.162	1	-170 to -160	offset	x	x
23	172.6	46.1	0.161	1	-20 to -10	offset	x	x
24	112.3	57.8	0.159	9	-140 to -50	both	5.1	1
25	62.6	42.9	0.157	1	-20 to -10	offset	x	x
26	165.6	47.9	0.155	1	-20 to -10	on	x	x
27	65.0	37.1	0.155	6	-160 to -100	both	x	x
28	68.6	37.1	0.150	3	-160 to -130	offset	x	x

Table 1—Continued

No.	l	b	Temp.(mK)	No. Maps	Vel. (km/s)	Offset or On	Section	Figure
29	93.2	66.6	0.150	1	-10 to 0	offset	5.6	9
30	121.6	56.8	0.150	5	-160 to -110	offset	5.3	3
31	113.4	66.4	0.149	1	-20 to -10	offset	5.5	7
32	89.3	34.5	0.146	7	-200 to -130	on	5.4	4, 5, 6
33	94.6	38.6	0.143	4	-190 to -160	offset	5.4	4
33	-130 to -120	offset	5.4	4
...	total 103

Table 2. COMPARISON AREA ASSOCIATIONS

No.	l	b	True l	Temp. (mK)	No. Maps	Vel. (km/s)	Offset or On
(1)	(2)	(3)	(4)	(5)	(6)	(7)	(8)
1	139.6	40.1	259.6	0.227		none	none
2	174.4	56.8	294.4	0.223	3	-30 to -20	offset
2	0.223	...	-20 to -10	offset
2	0.223	...	60 to 70	offset
3	160.3	62.9	280.3	0.218	none	none	none
4	176.1	53.0	296.1	0.212	none	none	none
5	140.3	41.5	260.3	0.202	none	none	none
6	172.3	59.5	292.3	0.199	none	none	none
7	174.0	50.5	294.0	0.182	none	none	none
8	177.2	57.6	297.2	0.182	1	-20 to -10	offset
9	168.1	67.4	288.1	0.180	none	none	none
10	171.6	56.3	291.6	0.179	none	none	none
11	118.1	57.0	238.1	0.175	1	-20 to -10	offset
12	159.6	50.0	279.6	0.172	1	-40 to -30	offset
13	169.5	46.5	289.5	0.172	none	none	none
14	174.7	48.2	294.7	0.172	none	none	none
15	101.8	59.5	221.8	0.169	1	-30 to -20	offset
16	78.4	55.9	198.4	0.168	3	-60 to 30	offset
17	82.3	55.7	202.3	0.168	2	-60 to -40	offset
18	165.7	64.8	285.7	0.168	none	none	none

Table 2—Continued

No.	l	b	True l	Temp. (mK)	No. Maps	Vel. (km/s)	Offset or On
19	91.5	36.7	211.5	0.166	2	-50 to -30	offset
20	170.2	54.5	290.2	0.165	1	-30 to -20	offset
21	135.4	51.1	255.4	0.164	none	none	none
22	151.2	48.8	271.2	0.162	2	40 to 60	offset
23	172.6	46.1	292.6	0.161	none	none	none
24	112.3	57.8	232.3	0.159	1	-20 to -10	offset
25	62.6	42.9	182.6	0.157	none	none	none
26	165.6	47.9	285.6	0.155	1	-10 to 0	offset
27	65.0	37.1	185.0	0.155	none	none	none
28	68.6	37.1	188.6	0.150	none	none	none
29	93.2	66.6	213.2	0.150	none	none	none
30	121.6	56.8	241.6	0.150	1	-20 to -10	offset
31	113.4	66.4	233.4	0.149	none	none	none
32	89.3	34.5	209.3	0.146	none	none	none
33	94.6	38.6	214.6	0.143	1	-40 to -30	offset
...	total 21

Table 3. Numbers of Associations Between HI and *WMAP* Structure

Class	Predicted	Observed	Predicted	Observed
...	Target Area	...	Comparison Area	...
Direct association	0.4	9 (+2)	0.2	0
(within 0.2°)
Close offset	5.1	12	5.9	5
...	(within 1°- see text)	...	(within 1.5°- see text)	

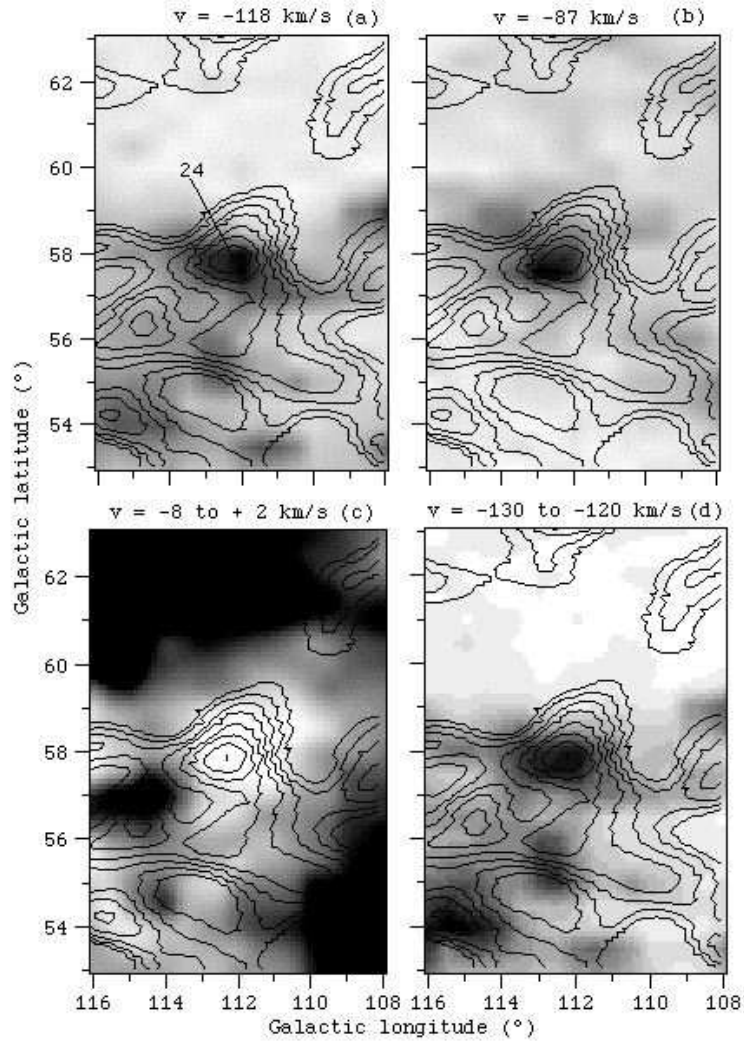


Fig. 1.— Source 24 at $(l, b) = (112.^{\circ}3, 57.^{\circ}8)$ at the center of the map showing overlapping HI (inverted gray scale) at the velocities indicated and *WMAP* structure (contours from +0.04 in steps of 0.02 mK) overlain.

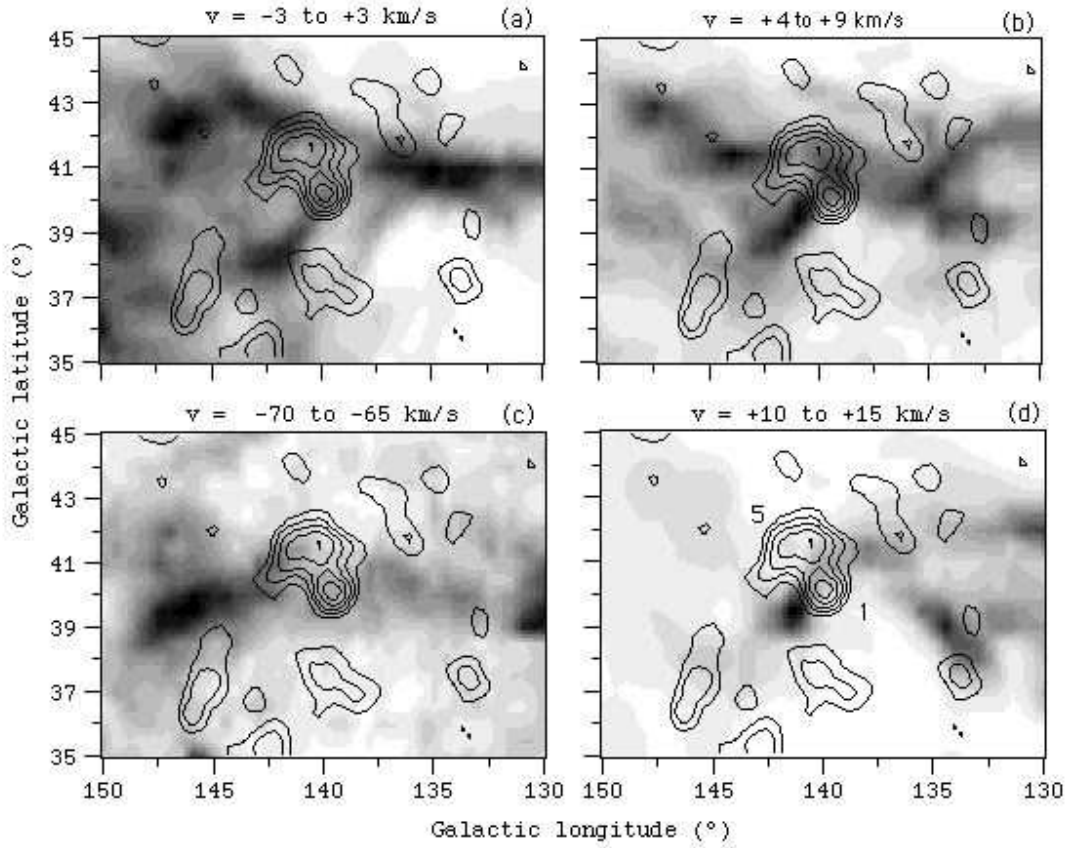


Fig. 2.— Sources 1 and 5 centered at $(l,b) = (140^\circ, 40^\circ)$ marked in (d). Four images of the HI filaments at the velocities indicated are plotted as inverted gray-scale with the overlain *ILC* contours indicating the continuum emission from 0.04 mK in steps of 0.04 mK.

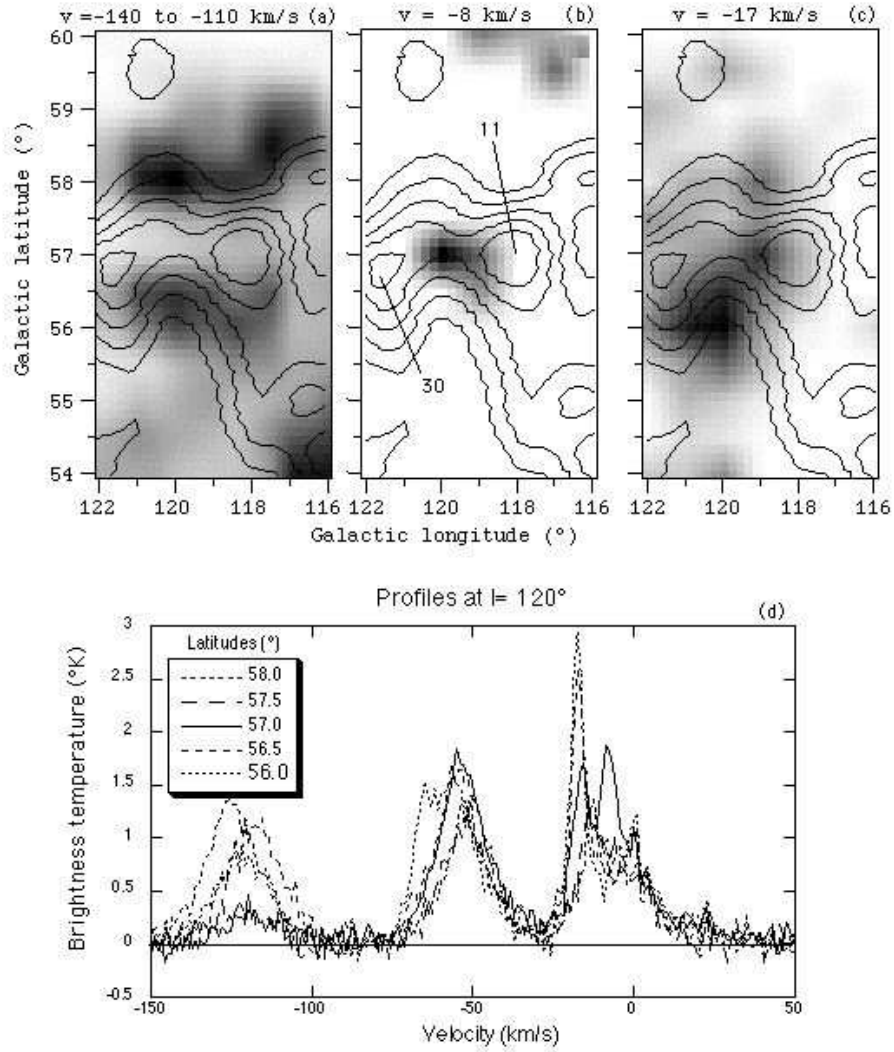


Fig. 3.— Sources 11 & 30 centered at $(l, b) = (120^\circ, 57^\circ)$ showing the relationship between HI features at the velocities indicated with the *WMAP* continuum emission contours (from 0.02 mK in steps of 0.03 mK) overlain. Continuum bridges the gap between the two sources. Frame (d) shows several HI emission profiles at the positions indicated.

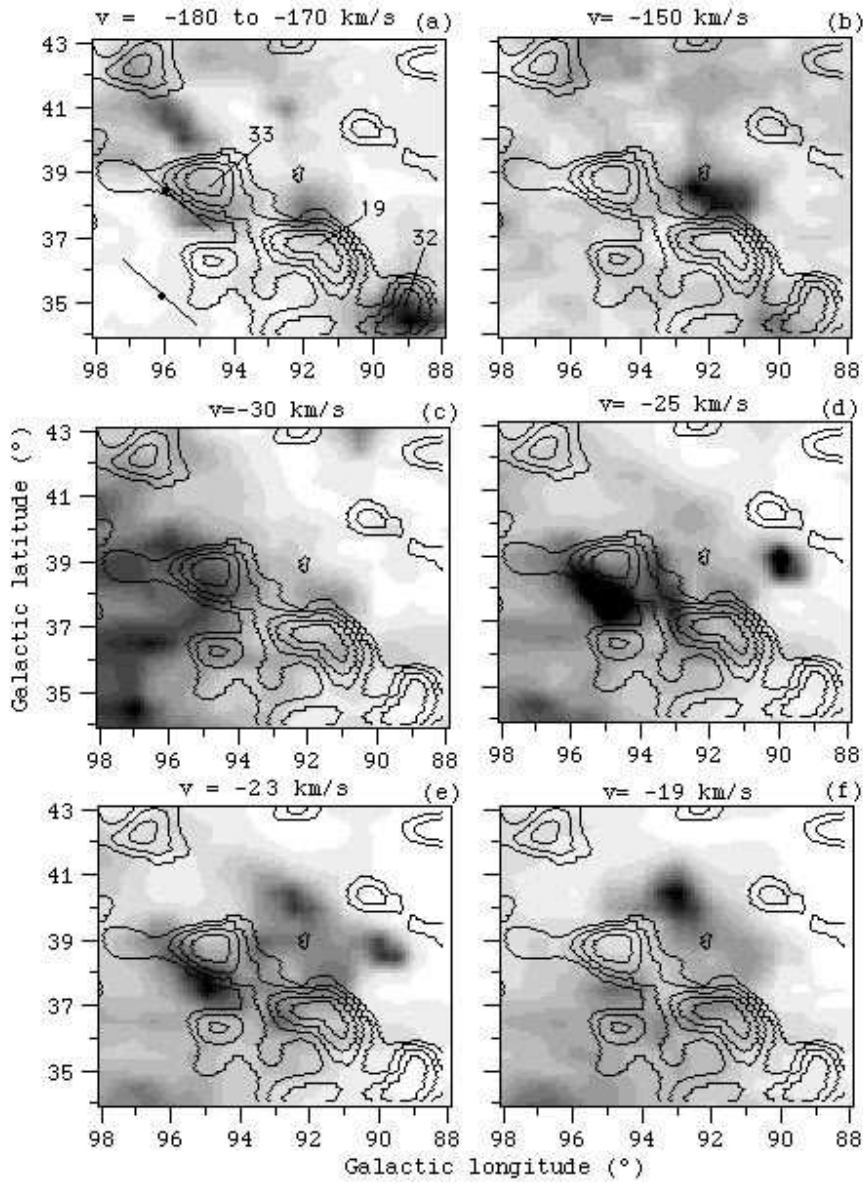


Fig. 4.— Sources 19, 32 & 33 centered at $(l, b) = (92^\circ, 37^\circ)$. The HI structures are shown as inverted gray-scale with the *WMAP* contours (from 0.03 mK in steps of 0.03 mK) overlain.

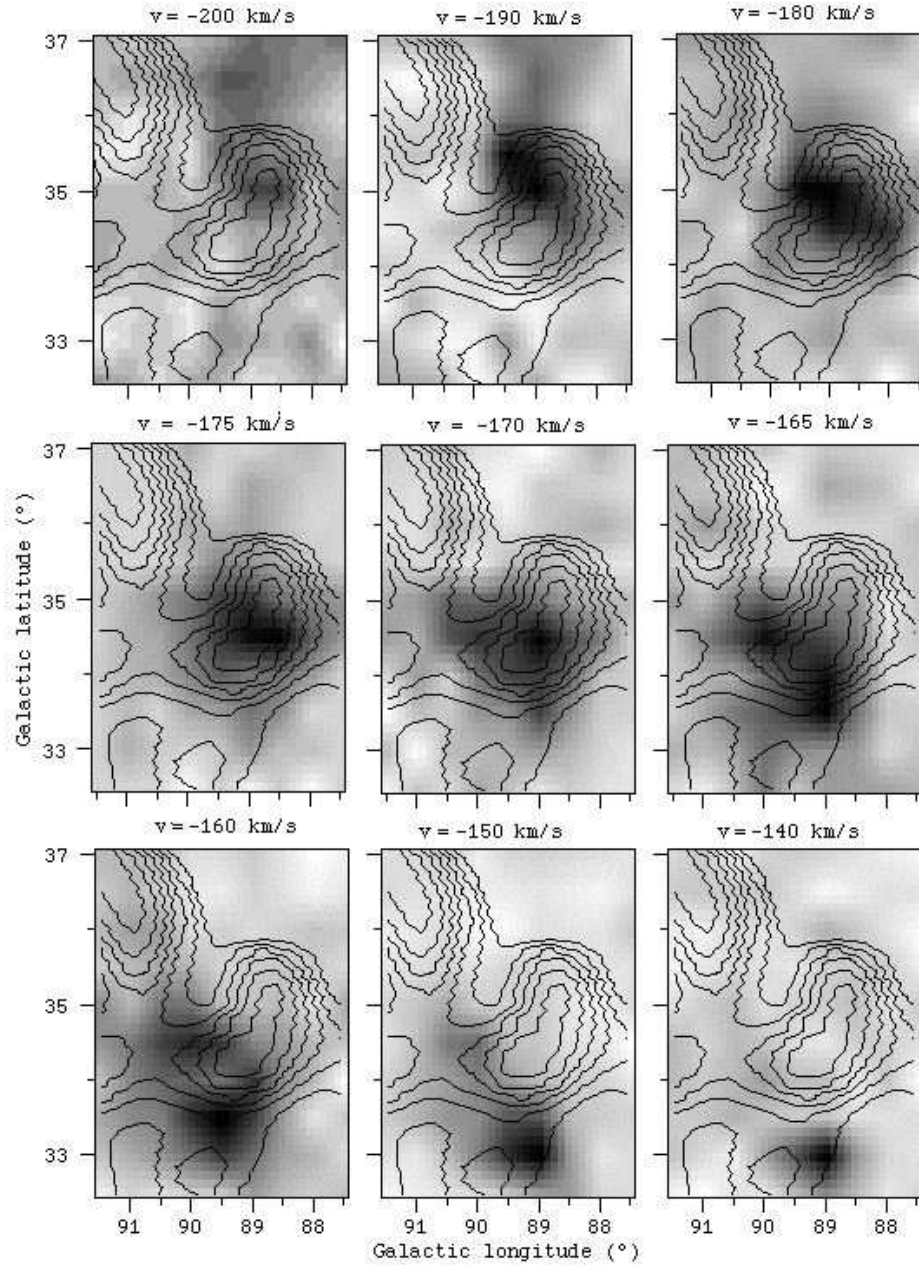


Fig. 5.— Continuum source 32 at $(l, b) = (89^\circ, 34.5^\circ)$ showing a direct relationship between a high-velocity HI structure (inverted gray-scale) and the *WMAP* emission peak (contour levels from 0.03 mK in steps of 0.02 mK).

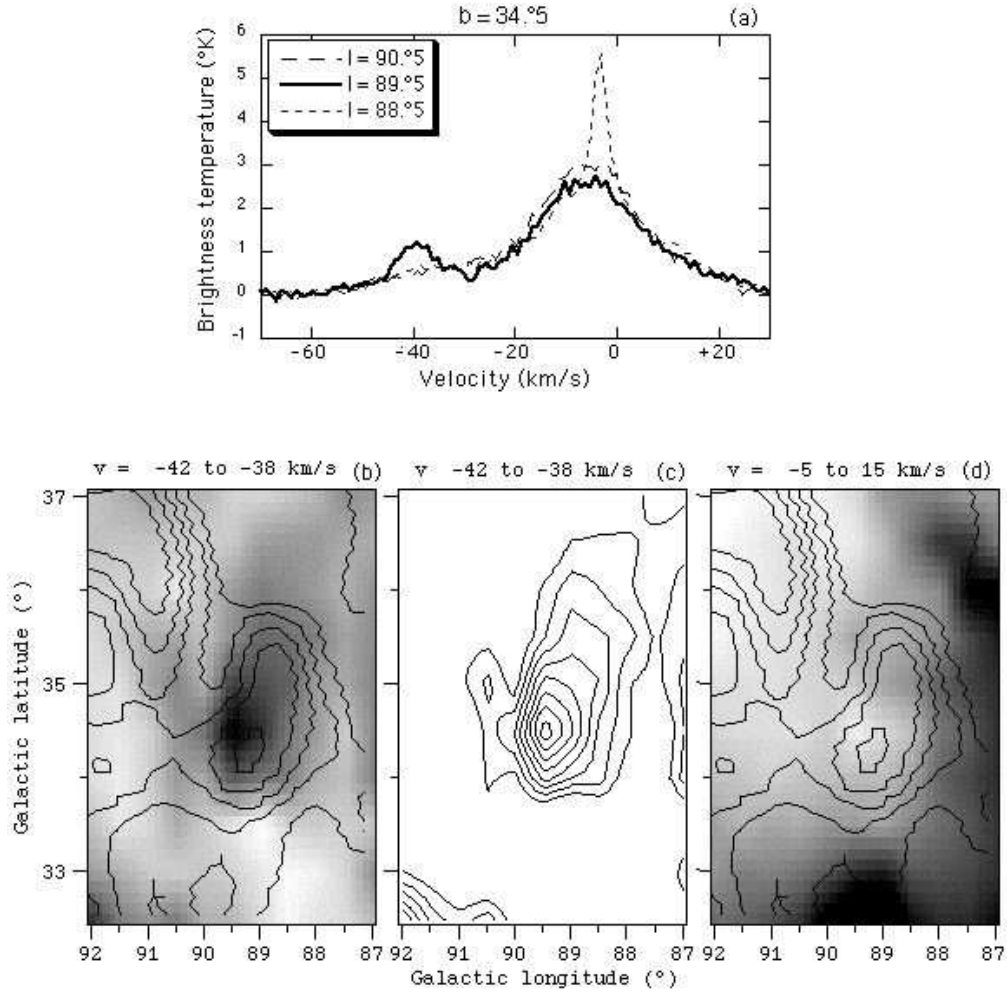


Fig. 6.— Further associations between the *WMAP* continuum source 32 and HI. See text for explanations.

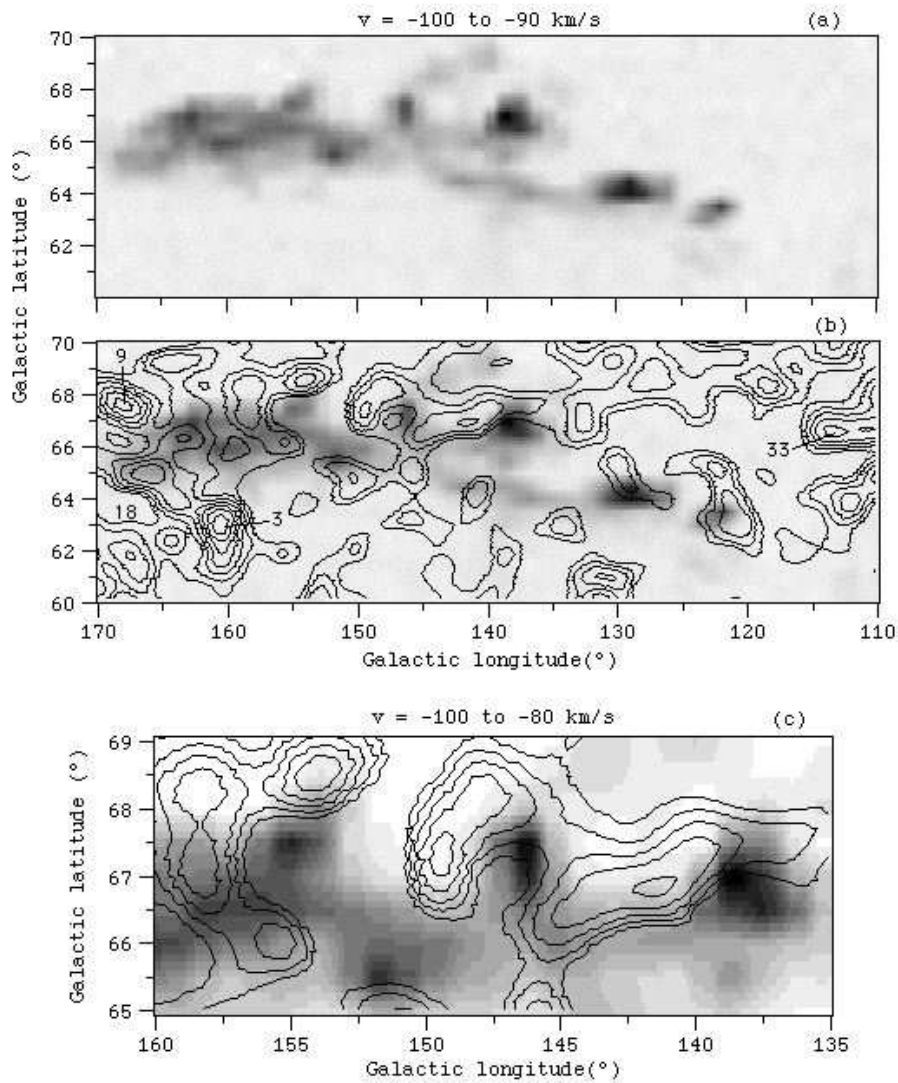


Fig. 7.— Continuum sources 3, 9, 18 & 31 in an area centered at $(l,b) = (140^\circ, 65^\circ)$. (a) An overview of HI emission (inverted gray-scale) from a corkscrew-like HI filament in the velocity range -100 to -90 km/s. (b) The same HI map as in (a) but with *WMAP* continuum emission contours (from 0.02 mK in steps of 0.02 mK) overlain. (c) A detailed view of the striking associations between HI and the continuum emission data for a section of the corkscrew area shown in (a).

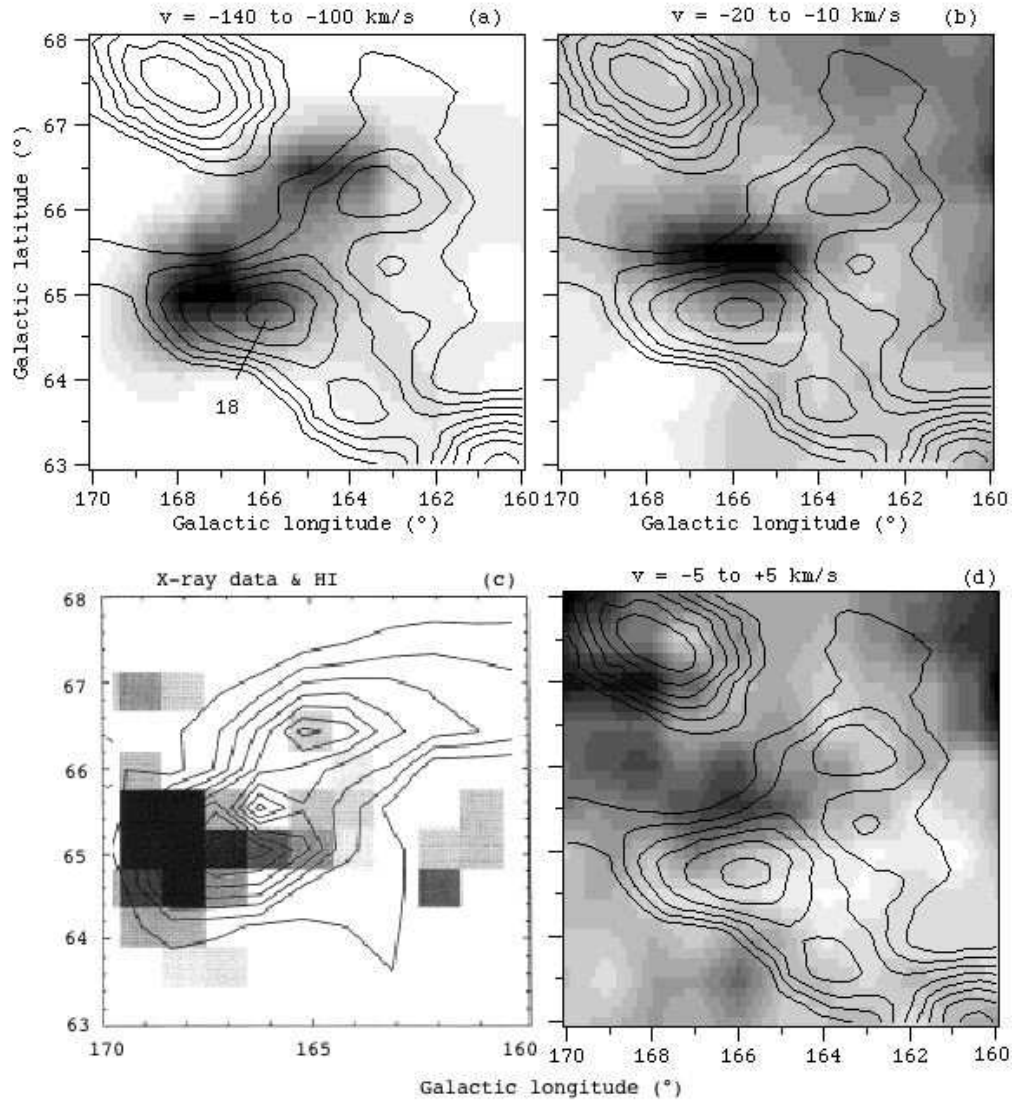


Fig. 8.— Source 18 at $(l, b) = (165.^{\circ}7, 64.^{\circ}8)$ located in the complex seen in Fig. 7. (a) (b) & (d) are inverted gray-scale images of the HI emission at the velocities indicated. (c) The location of a soft X-ray excess emission (pixels) with respect to HVC MI contours (see text).

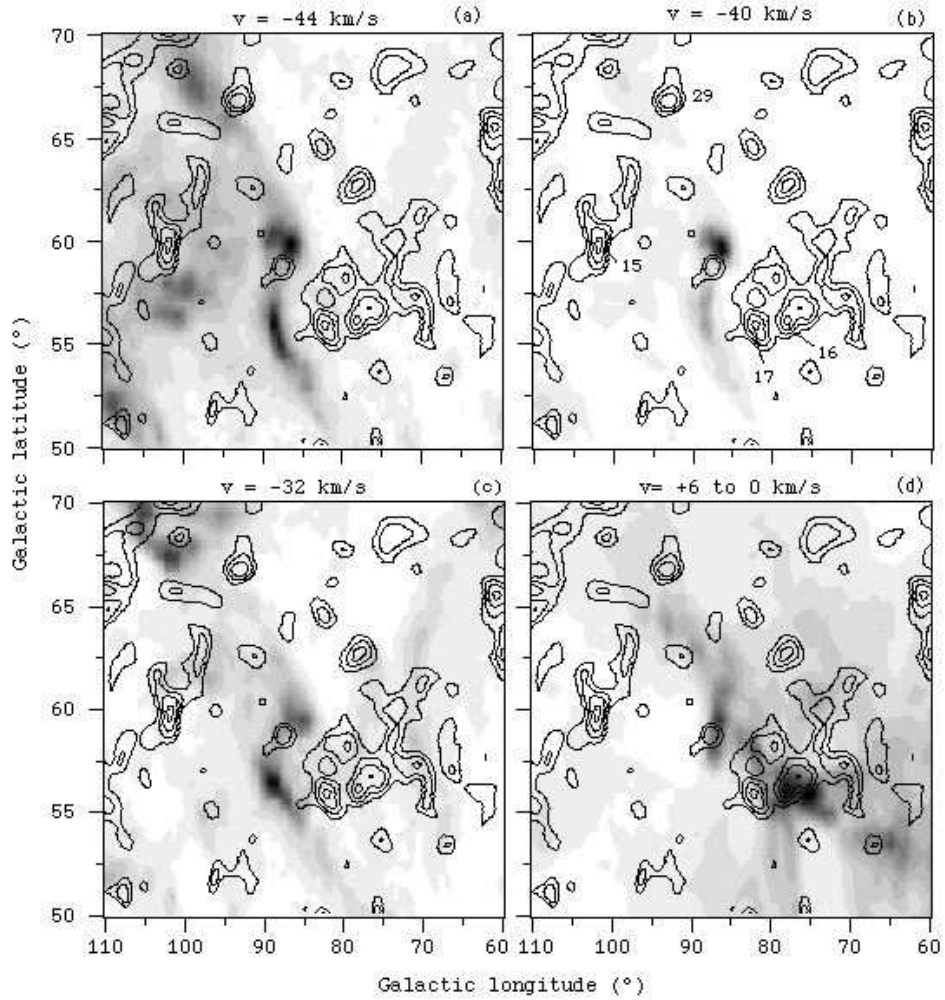


Fig. 9.— Examples of the relationship between HI at the velocities indicated and *WMAP* emission contours (from 0.04 mK in steps of 0.04 mK) for structure in an area centered at $(l, b) = (85^\circ, 60^\circ)$. This includes continuum sources 15, 16, 17 & 29 (see text).

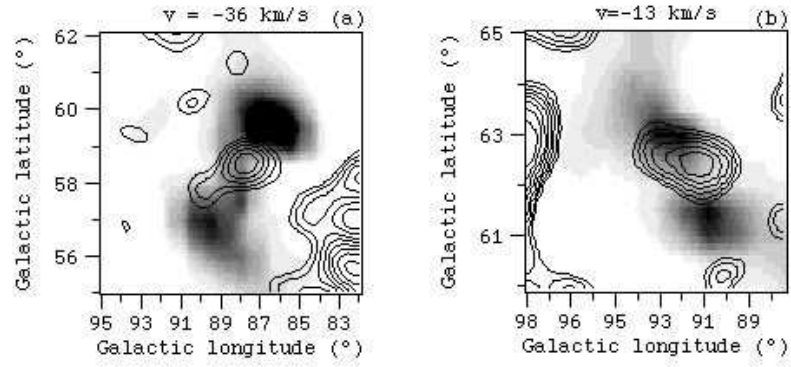


Fig. 10.— Two pairs of HI peaks found in the area described in Fig. 9. at the velocities indicated. A continuum peak is found in between each pair (see text). These associations lie on the axis of the major filament seen in Fig. 9a.

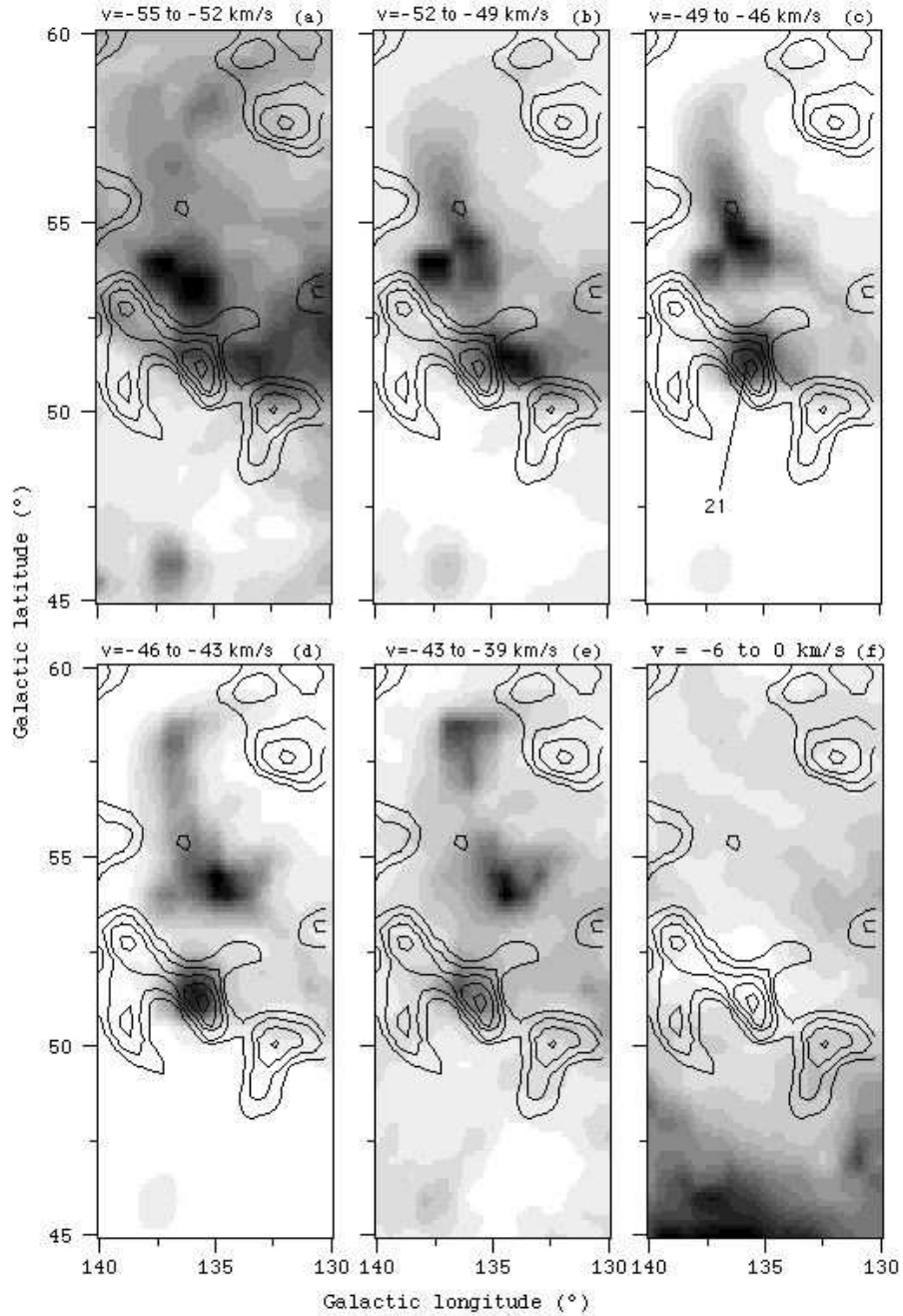


Fig. 11.— Continuum source 21 at $(l, b) = (135.^{\circ}4, 51.^{\circ}1)$, which coincides with the southern component of a complex of HI seen here over a velocity range from -55 to -39 km/s. The *WMAP* continuum contours (from 0.03 mK in steps of 0.03 mK) are overlain. In (f) a lack of HI emission at low velocities is found at the location of the IV HI peak associated with the continuum source 21 in the other frames.